Dear Author,

Please, note that changes made to the HTML content will be added to the article before publication, but are not reflected in this PDF.

Note also that this file should not be used for submitting corrections.

Carbon xxx (2015) 1–6

Contents lists available at ScienceDirect

Carbon

journal homepage: www.elsevier.com/locate/carbon

The mechanical properties of energetically deposited non-crystalline carbon thin films

M. Kracica [a,*], C. Kocer [d], D.W.M. Lau [a], J.G. Partridge [a], J.E. Bradby [b], B. Haberl [c], D.R. McKenzie [d], D.G. McCulloch [a]

[a] School of Applied Sciences, RMIT University, Victoria 3001, Australia
[b] Department of Electronic Materials Engineering, Research School of Physics and Engineering, The Australia National University, Acton 2601, Australia
[c] Chemical and Engineering Materials Division, Neuron Sciences Directorate, Oakridge National Laboratories, Oakridge, TN 37831, USA
[d] School of Physics, The University of Sydney, New South Wales 2006, Australia

ARTICLE INFO

Article history:
Received 14 August 2015
Received in revised form
26 October 2015
Accepted 27 October 2015
Available online xxx

ABSTRACT

The mechanical behaviour of carbon films prepared with a variety of densities and microstructures was investigated using nanoindentation. Deposition energies between 25 and 600 eV and temperatures in the range 25–600 °C were used. Films prepared at low temperatures and moderate energies were amorphous with a high density. Finite element methods were used to model the stress fields, reproduce the indentation behaviour and evaluate elastic properties. Young's moduli up to 670 GPa and a low Poisson's ratio of ~0.17 were found, comparable to polycrystalline cubic boron nitride, one of the hardest materials known. Films with the same density did not always show the same behaviour, emphasising the role of microstructure in determining mechanical response. Extended graphite-like regions within the films grown at high energy and high temperature, observed in transmission electron microscopy caused plastic deformation and failure to recover after a complete indentation cycle. At low deposition energies, the graphite-like regions were smaller in size causing plastic deformation but with complete recovery after indentation.

© 2015 Published by Elsevier Ltd.

1. Introduction

Carbon coatings exhibit wear-resistance, low-friction, biocompatibility and high durability in chemically harsh conditions [1–4]. The main application for non-crystalline carbon thin films is in wear protection [1,4–6]. If the microstructure contains a high proportion of diamond-like (sp^3) bonds, the film is dense and mechanically hard. For example, tetrahedral amorphous carbon (ta-C) is an amorphous form of carbon with up to 85% sp^3 bonds and is one of the hardest known covalent network solids [7]. In contrast, films containing a low fraction of sp^3 bonds show a lower modulus but exhibit a high degree of elastic recovery from large deformations [4]. This property, also observed in glassy carbon [8] is known as aneslasticity [9,10]. Anelasticity arises from the fact that the graphene sheet is the strongest two dimensional structure known and can exhibit a shape memory effect [11]. In terms of non-crystalline carbon films, the relationship between the microstructure and any recovery is not presently understood.

There is a wide variability in the reported elastic modulus (100–800 GPa [4,12–14]) and hardness (5–80 GPa [4,12–14]) of non-crystalline carbon films, with the latter based largely on empirical models. In general, it has been reported that the hardness and/or modulus of carbon films correlates simply with the fraction of sp^3 bonds or density [4,15,16]. However, the microstructure and in particular the arrangement of any layered graphitic structures, may also influence the mechanical properties. There is currently no detailed study of the relationship between microstructure and mechanical properties in non-crystalline carbon thin films. This knowledge would enable the selection of carbon coatings optimised for particular tribological applications.

Here, we investigate the mechanical properties of non-crystalline carbon films with different densities and microstructures. The film characteristics were controlled by adjusting the average energy of the depositing flux and the growth temperature within a filtered cathodic vacuum arc (FCVA) deposition system [17,18]. The microstructure of the films was characterised using transmission electron microscopy (TEM) and electron energy loss

* Corresponding author.
E-mail address: masturina.kracica@rmit.edu.au (M. Kracica).

http://dx.doi.org/10.1016/j.carbon.2015.10.085
0008-6223/© 2015 Published by Elsevier Ltd.

UNCORRECTED PROOF

Please cite this article in press as: M. Kracica, et al., The mechanical properties of energetically deposited non-crystalline carbon thin films, Carbon (2015), http://dx.doi.org/10.1016/j.carbon.2015.10.085

spectroscopy (EELS). Nanoindentation was used in combination with Finite Element Modelling (FEM) to probe the mechanical properties of the films. Measurements of the reduced elastic modulus, average energy dissipation and residual penetration depth following indentation revealed the relationships between the mechanical properties, density and microstructure of the films.

2. Method

Carbon films were deposited using a FCVA system equipped with a double bend magnetic filter to minimise the incorporation of macro particles into the growing film. A base pressure of less than 2×10^{-5} Torr was established before each deposition. These were performed by ablating the 99.9% pure graphite source with an arc current of ~60 A. Films with thicknesses between 100 and 150 nm were deposited onto n-type conductive 6H–SiC and Si substrates. Previous nanoindentation experiments performed on carbon films supported by Si revealed that the Si deformed significantly under moderate loads [19]. For this reason, 6H-SiC was chosen for all nanoindentation measurements as a precautionary measure due to its relatively high elastic constant (400 GPa) and because no phase changes occur during indentation (unlike in Si [20]). Samples were mounted onto a bias compatible substrate heater/holder, and depositions were performed using biases from 0 V (earthed) to 600 V and substrate temperatures from 30 °C to 600 °C. The depositing carbon flux in the FCVA system is fully ionised [17,18] so the average deposition energy can be determined from the bias voltage, average charge state of the plasma (1+ for carbon [17]) and the energy of the carbon flux (measured to be ~20 eV in our system [17]).

The microstructure of the films was studied using a JEOL 2010 TEM operated at 200 kV. EELS was performed using a Gatan imaging filter to obtain the mass density. Films were prepared for TEM by sacrificially etching the Si substrates. A cross-section TEM sample of one of the films was also prepared by mechanical polishing and ion beam thinning. Low loss EELS spectra were collected from each film and deconvoluted for multiple scattering using the Fourier log method. The sample densities were calculated from the plasmon peak positions, assuming a free electron model with four valence electrons and an effective mass of 0.88 m_e (where m_e is the electron mass at rest) [17,21,22].

Nanoindentation experiments were performed using a Hysitron TI-950 nanoindenter fitted with a Berkovich tip. The effective radius of the tip, measured using a scanning electron microscope, was ~220 nm. A maximum load of 200 μN was applied using loading/unloading segment times of 10 s to produce load–displacement curves [23]. The maximum load was chosen to ensure the maximum penetration depth was <15% of the film thickness to minimise substrate effects [24]. No hold period at maximum load was used to avoid recovery effects due to the anelasticity of the films. Due to this behaviour, the standard Oliver–Pharr method for measuring the hardness and modulus of the films was not applicable [25–27]. Instead, the following analyses were applied in the purely elastic regime. The initial loading portion (up to ~50 μN) was fitted using the Hertzian equation [23,26,28] to calculate the reduced elastic modulus (E_r). For the plastic–elastic behaviour, the energy dissipation (E_d) during indentation can be extracted using:

$$E_d = (U_{load} - U_{unload})/U_{load} \quad (1)$$

where U_{load} and U_{unload} are the areas under the loading and unloading curves, respectively [25].

Finite element modelling was used to model experimental force-displacement curves for four representative carbon films with different microstructures. A 2-D axisymmetric model was constructed using the finite element software ANSYS [29]. Fig. 1a shows the FEM model used. The Berkovich tip was approximated with a spherical tip of radius 220 nm, which is valid for small penetration depths. In the finite element model, the SiC substrate was 400 × 400 nm with varying film thicknesses. In order to accurately model the indentation process and to optimise the finite element calculations, a mesh size of <10 nm was refined. The indentation simulations were performed by applying loads of up to 200 μN in the elastic regime. The values of Young's modulus (E) and Poisson's ratio (υ) of the diamond indenter and SiC substrate were 1100 GPa and 0.07 [30] and 400 GPa and 0.19, respectively [31]. Estimates of E for the four carbon films were obtained from the experimental measurements of E_r and values of υ between 0.19 and 0.28 [4,12]. These starting values of E and υ were used in the FEM model in order to obtain an initial simulated load–displacement curve and then adjusted until the simulated load–displacement curve matched the initial part of the loading segment obtained experimentally. Fig. 1b and c shows contour plots of the hydrostatic pressure at maximum load for a high modulus (E = 670 GPa) and low modulus (E = 75 GPa) carbon film. The plots show that the stress field caused by the indentation is mainly contained within

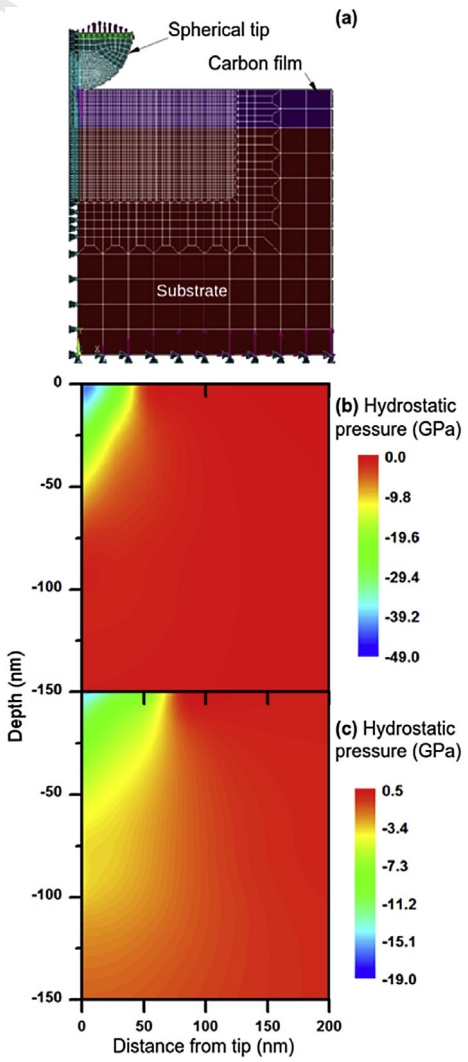

Fig. 1. (a) The FEM model used to simulate the indentation process. Two examples of the stress field for carbon films with (b) high modulus (E = 670 GPa) and (c) low modulus (E = 75 GPa) at the maximum load of 200 μN. (A color version of this figure can be viewed online.)

UNCORRECTED PROOF

Please cite this article in press as: M. Kracica, et al., The mechanical properties of energetically deposited non-crystalline carbon thin films, Carbon (2015), http://dx.doi.org/10.1016/j.carbon.2015.10.085

the thin film at the maximum experimental load (200 μN).

3. Results and discussion

Fig. 2 shows the density of FCVA-fabricated carbon films as a function of ion energy and substrate temperature. This contour plot is based on our previous work [17] and is included here to assist in showing the relationship between the density of the films and their mechanical properties. High density films are produced with ion energies of 50–400 eV and substrate temperatures of up to 250 °C. This region corresponds to the conditions under which high compressive stresses lead to the formation of ta-C with densities up to 3.0 g/cm^3 [17]. The highest density material, which contains up to ~85% sp^3 bonding, is formed when depositing onto a substrate at a temperature of ~150 °C and with ion energies of ~95 eV [17]. It is well established that the microstructure of these high density films is amorphous [7,17,32,33]. In films deposited at room temperature, the density decreases at both high and low ion energies. At lower deposition energies, ions have insufficient energy to create the compressive stress required to form diamond-like bonds [17,32,33]. At higher ion energies, structural relaxations promote lower energy sp^2 bonding and a lower density. The highest density material (~3.1 g/cm^3) was formed at ~150 °C and ion energies between 100 and 200 eV. At temperatures above ~250 °C, the film density (~2.2 g/cm^3) is relatively insensitive to changing ion energy. This density is close to that of crystalline graphite and previous work has shown that these films have a high proportion of sp^2 bonding [17,33]. However, within this constant density region, a range of microstructures has been reported [4,34–36].

Fig. 3a shows the load–displacement curves from samples prepared with 45 eV ion energy at temperatures of 25, 200 and 600 °C. The sample prepared at room temperature is ta-C with a density of ~3.0 g/cm^3 (Fig. 2). The load portion of the curve overlays with the unload portion, showing that there was only elastic deformation with no significant plastic deformation. A E_r of 370 GPa was calculated from this curve. The recovery from the elastic deformation was complete, with no residual indent impression remaining. This type of elastic behaviour is typical of ta-C [4,37]. A lower E_r (200 GPa) is calculated from the load portion of the curve from the sample prepared at 200 °C. Hysteresis exists between the load and unload curves and a very small residual indent impression remains at the completion of the cycle. When the deposition temperature was raised to 600 °C, E_r decreases to ~100 GPa and the hysteresis increases. However, there is still little or no residual

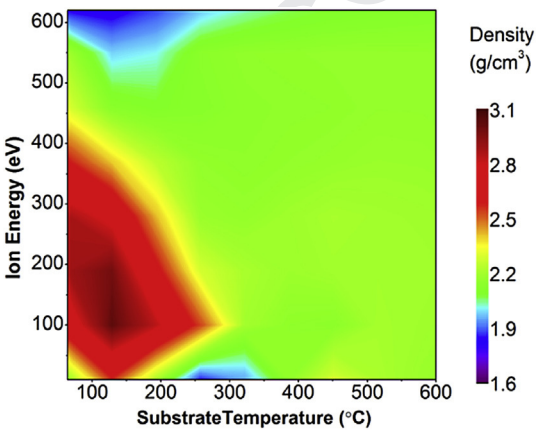

Fig. 2. Contour plot (adapted from Ref. [17]) showing the density of carbon thin films deposited from the FCVA as a function of average ion energy and substrate temperature. (A color version of this figure can be viewed online.)

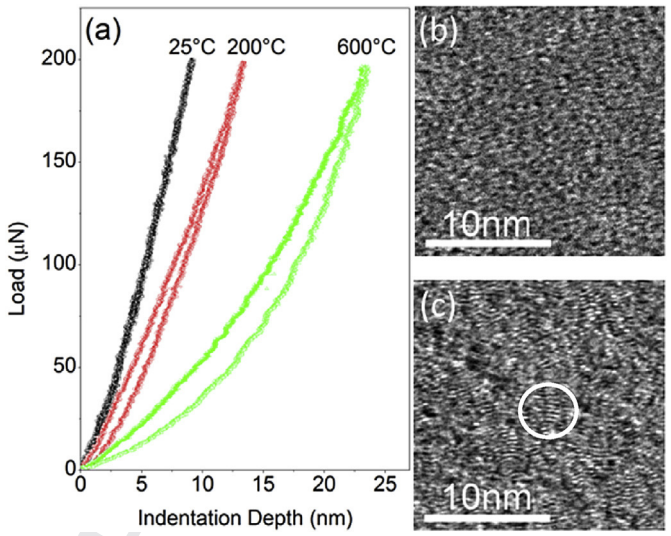

Fig. 3. (a) Typical load-displacement curves of carbon samples deposited at ion energy of 45 eV and substrate temperatures 25, 200 and 600 °C. Plan view TEM images of the samples deposited at 200 and 600 °C are shown in (b) and (c). A small graphitic region is circled in (c). (A color version of this figure can be viewed online.)

indent impression. The existence of load–unload hysteresis with no residual indent impression is characteristic of these samples and resembles the previously reported behaviour of glassy carbon [9].

The recovery was time dependent but in the cycle time used in these experiments (20 s), it was complete.

The load–unload curve exhibited by the sample prepared with 45 eV ion energy at 25 °C (Fig. 3a) is consistent with high modulus ta-C which has a dense sp^3 bonded amorphous microstructure (not shown). Plan view TEM images of the samples deposited at elevated temperatures are shown in Fig. 3b and c. The microstructure of the sample prepared at 200 °C is still largely amorphous but with lower density (2.5 g/cm^3), this sample contains more graphite-like bonds and therefore has a lower modulus, as shown in its load–unload behaviour (Fig. 3a). The load–unload hysteresis can be explained by deformation occurring in the sp^2 bonded component of the film. In the film deposited at 600 °C (Fig. 3c), small graphitic regions are clearly discernible (see circled region in Fig. 3c).

These graphitic regions are likely to be responsible for the increased load–unload hysteresis. Due to their small size (<2 nm), however, they do not permanently deform and the film completely recovers. The small size of these graphitic regions is associated with the small thermal spike volumes of 45 eV impacts. The diameter of the molten volume of such a spike is expected to be less than 2 nm [38], consistent with our observations.

Fig. 4a shows the load–displacement curves from samples deposited with 600 eV ion energy and deposition temperatures of 25, 400 and 600 °C. All three exhibit larger hysteresis compared to the samples prepared at lower energies (Fig. 3a). In addition, for these samples the recovery is not complete after the load-unload cycle, resulting in a residual indent impression. The samples deposited at 400 and 600 °C contain larger graphite-like regions, up to 10 nm in size (Fig. 4b and c). The larger correlated regions are consistent with the larger thermal spike volumes produced by 600 eV impacts. These larger graphite-like structures are more readily deformed due to slippage over larger distances and do not recover in the 20 s cycle time.

A cross-sectional TEM image of a sample prepared at 600 °C and 600 eV is shown in Fig. 5a with the substrate visible at the bottom of the image. A selected area diffraction pattern from the film is shown in Fig. 5b. The intense spots aligned parallel to the substrate

Please cite this article in press as: M. Kracica, et al., The mechanical properties of energetically deposited non-crystalline carbon thin films, Carbon (2015), http://dx.doi.org/10.1016/j.carbon.2015.10.085

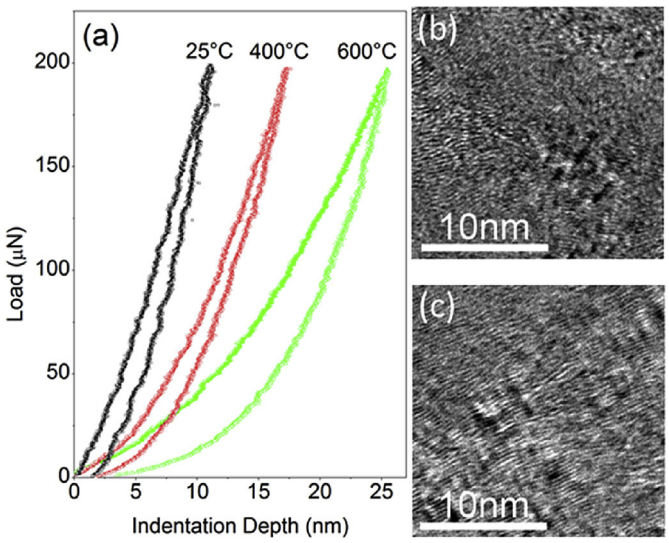

Fig. 4. (a) Typical load-displacement curves of samples prepared with 600 eV ion energy and with deposition temperatures of 25, 400 and 600 °C. The microstructure of the films deposited at 400 and 600 °C are shown in the TEM images (b) and (c) respectively. (A color version of this figure can be viewed online.)

have been indexed to {002} graphite reflections. These indicate that the film contains oriented graphite-like regions with layers aligned perpendicular to the substrate. This type of preferred orientation has been reported previously and was attributed to a response of the anisotropic graphite crystallites to the compressive biaxial stress field present during growth at higher energies (>600 eV) and at elevated temperatures beginning from low energies [17,32]. These oriented graphitic regions are present through the full depth of the sample, as shown in the dark-field image taken from one of the {002} reflections (Fig. 5b).

The large indent impression observed after a load–unload cycle shows this microstructure is susceptible to permanent deformation.

Fig. 6 shows contour plots of (a) E_r, (b) the residual indent impression after a complete cycle and (c) E_d for a large number of samples with a range of deposition temperatures and ion energies.

In nanoindentation measurements, the hardness is usually defined by the maximum load and the projected area of the residual indent impression [23,26]. As mentioned earlier, the almost full recovery observed following indentation of most of these samples prevented the application of this standard approach. Films with the highest E_r of up to ~400 GPa are formed under conditions which produce the highest density (Fig. 2). This value is in the range 350–700 GPa previously reported for ta-C [12]. Generally, as the density of the films reduces so does E_r, consistent with previous studies [4,39,40]. However, this is not always the case. At high deposition temperatures and/or energies, films with similar densities (the green region corresponding to ~2.2 g/cm^3 shown in Fig. 2) have different E_r.

These changes in E_r are attributed to the different film microstructures as discussed above. The samples deposited at elevated temperatures with significant levels of sp^2 bonding exhibit the lowest E_r. The plastic deformation as evidenced by the residual indent impression (Fig. 5b) is larger at high energies due to the larger thermal spikes creating larger correlation distances. This measure does not follow the same trend as E_r. Instead, a maximum in residual indent impression occurs at the highest temperatures and energies, while E_r is constant with energy at the highest temperature. This behaviour is attributed to the increasing crystalline volume fraction. Similarly, E_d is highest in samples prepared at both high temperatures and high energies, where the microstructures contain the largest ordered graphitic regions and thus follow the same trend as the residual impressions.

Fig. 7 shows the experimental and simulated load–displacement curves from four carbon films with different indentation behaviours. These simulations allow the Young's modulus (E) of the films to be determined. This is different from the reduced elastic modulus (E_r) shown in Fig. 6a which is the composite modulus of the indenter and specimen. Fig. 7a shows the result for a high modulus ta-C sample prepared at an energy of 45 eV and a substrate temperature of 25 °C. The correspondence between the simulated and experimental curves shows that the film exhibits elastic behaviour even at the highest load. E of 670 GPa and υ of 0.12 were found to provide the best fit with experiment. These values are similar to those reported by Ferrari [12] for ta-C measured using surface acoustic waves (Brillouin scattering). To put this value in perspective, the values of E and υ of polycrystalline cubic boron nitride (one of the highest modulus non-crystalline material

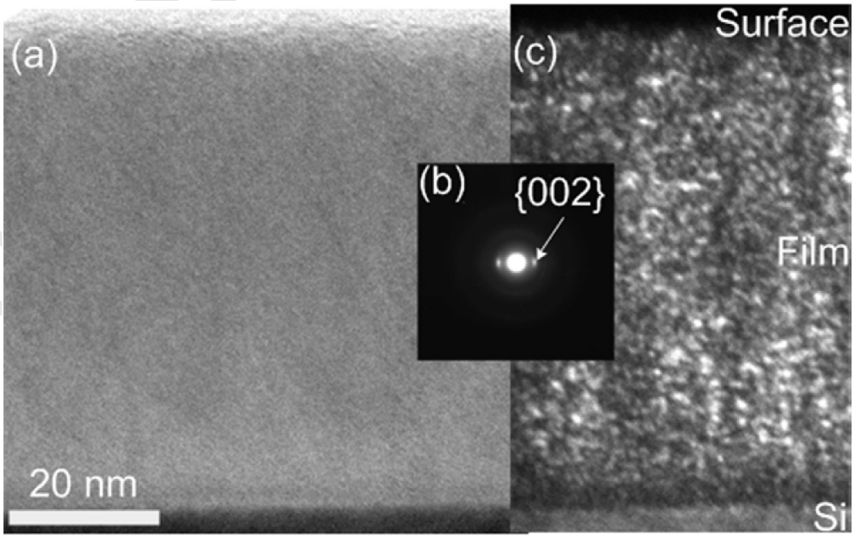

Fig. 5. (a) The cross-sectional TEM image of a sample prepared at 600 °C and 600 eV, with the substrate at the bottom. (b) A selected area diffraction pattern from the film, with the bright diffraction spots indexed to graphite. (c) The dark field image from the same area as (a) collected from one of the {002} diffraction spots.

Please cite this article in press as: M. Kracica, et al., The mechanical properties of energetically deposited non-crystalline carbon thin films, Carbon (2015), http://dx.doi.org/10.1016/j.carbon.2015.10.085

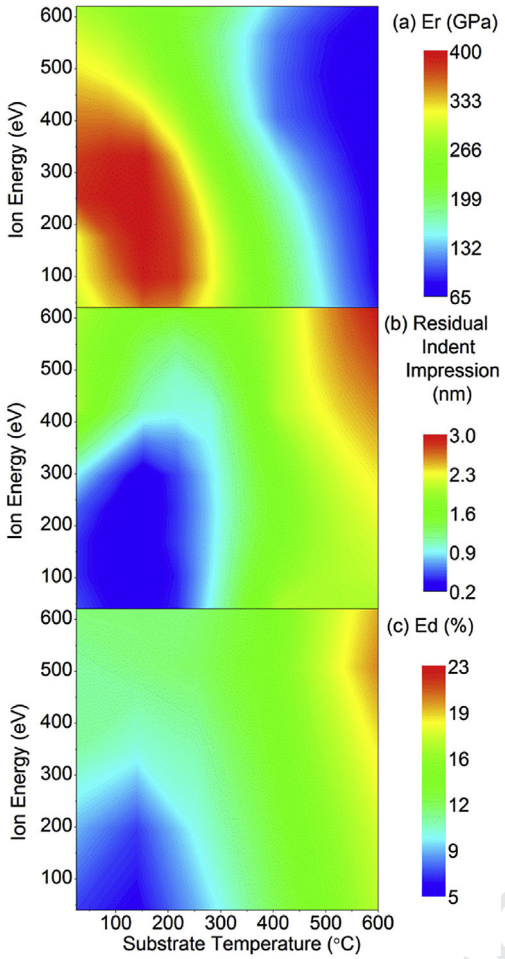

Fig. 6. (a) The reduced elastic moduli (E_r), (b) residual impression after indentation and (c) energy dissipation (E_d) measured in carbon films deposited with different average ion energy and substrate temperature. (A color version of this figure can be viewed online.)

known) are 630–770 GPa and 0.14–0.18 respectively [41,42]. Fig. 7b shows that the sample deposited at 45 eV and 200 °C (amorphous with a density of ~2.3 g/cm^3, see Fig. 3b) deviates from elastic behaviour at the point indicated by "A". E determined from the best fit of the FEM model was 235 GPa and υ is 0.17. These values reflect behaviour for a lower density disordered carbon. Fig. 7c and d shows results for films deposited at 600 °C, 45 eV and 600 °C, 620 eV respectively. The films exhibit increasing departures from purely elastic behaviour at lower loads (indicated by the points "A"). The best fit to the elastic portions of the curves gave E of 85 and 75 GPa, respectively. These lower values of E reflect the high levels of graphitic order in these films (see Figs. 3c and 4c).

There is a noticeable difference in the behaviours of the films in Fig. 7c and d. The film in Fig. 7c completely recovers from deformation even though there is considerable energy dissipation E_d. The ability of this film to recover all of the plastic flow (anelasticity) is remarkable and similar to that observed previously for glassy carbon [9,10]. We attribute this to the shape-memory of graphene sheets that are intertwined but do not form extended regions resembling graphite where permanent slippage is likely to occur. This latter behaviour is well illustrated in the TEM image of Fig. 3c, which has larger graphitic regions, resulting in the residual impression observed following indentation evident in Fig. 7d.

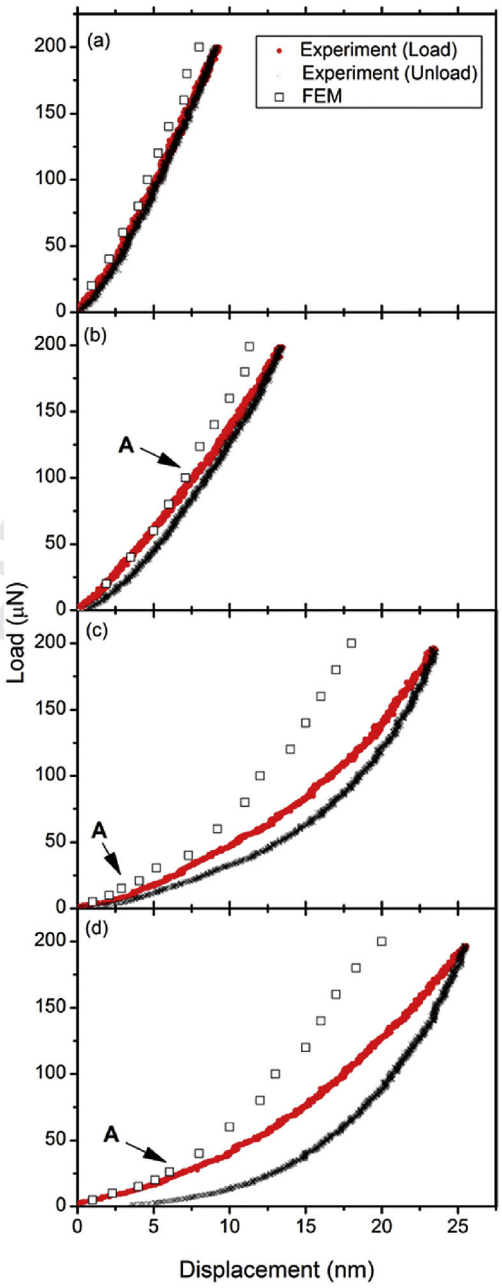

Fig. 7. Load-displacement characteristics obtained from non-crystalline carbon films deposited at (a) 25 °C, 45 eV (b) 200 °C, 45 eV (c) 600 °C, 45 eV and (d) 600 °C, 620 eV compared with simulated characteristics. The point 'A' indicates increasing departures from purely elastic behaviour at lower loads. (A color version of this figure can be viewed online.)

4. Conclusion

We have investigated the indention behaviour of carbon films prepared using energetic deposition at energies from 25 to 600 eV and temperatures from 25 to 600 °C. There is a wide range of indentation behaviour, even in films at the same densities. The behaviour is elastic in ta-C deposited with intermediate bias and low to medium temperature. Using finite element modelling, ta-C was found to have an E of 670 GPa, confirming that it has one of the highest Young's moduli known. The preparation of samples at low energy and moderate to high temperature results in anelastic behaviour, characterised by plastic deformation under load and full

UNCORRECTED PROOF

Please cite this article in press as: M. Kracica, et al., The mechanical properties of energetically deposited non-crystalline carbon thin films, Carbon (2015), http://dx.doi.org/10.1016/j.carbon.2015.10.085

recovery after indentation. In contrast, samples deposited at high energies over the full range of growth temperatures exhibit plastic behaviour without full recovery. These effects can all be explained in terms of the microstructure resulting from different thermal spike volumes at the different energies and the degree of graphite-like ordering determined by the growth temperature.

Acknowledgements

The authors acknowledge the scientific and technical assistance of the Microscopy and Microanalysis Facility at RMIT University (RMMF). Dr. Bianca Haberl gratefully acknowledges current funding Q1 from an Alvin M. Weinberg Fellowship (ORNL) and the Spallation Q2 Neutron Source (ORNL) , sponsored by the U.S. Department of Energy, Office of Basic Energy Sciences. The authors also thank Prof. Yeshayahu (Shay) Lifshitz for useful discussions.

References

[1] S.J. Bull, Tribology of carbon coatings: DLC, diamond and beyond, Diam. Relat. Mater. 4 (5–6) (1995) 827–836.
[2] R.K. Roy, K.-R. Lee, Biomedical applications of diamond-like carbon coatings: a review, J. Biomed. Mater. Res. Part B Appl. Biomaterials 83B (1) (2007) 72–84.
[3] H.O. Pierson, Handbook of Carbon, Graphite, Diamonds and Fullerenes: Processing, Properties and Applications, William Andrew, 2012.
[4] C.A. Charitidis, Nanomechanical and nanotribological properties of carbon-based thin films: a review, Int. J. Refract. Metals Hard Mater. 28 (1) (2010) 51–70.
[5] S.K. Field, M. Jarratt, D.G. Teer, Tribological properties of graphite-like and diamond-like carbon coatings, Tribol. Int. 37 (11–12) (2004) 949–956.
[6] K. Oguri, T. Arai, Tribological properties and characterization of diamond-like carbon coatings with silicon prepared by plasma-assisted chemical vapour deposition, Surf. Coatings Technol. 47 (1–3) (1991) 710–721.
[7] D.R. McKenzie, D. Muller, B.A. Pailthorpe, Compressive-stress-induced formation of thin-film tetrahedral amorphous carbon, Phys. Rev. Lett. 67 (6) (1991) 773–776.
[8] G.M. Jenkins, K. Kawamura, Polymeric Carbons—Carbon Fibre, Glass and Char, Cambridge University Press, Cambridge; New York, 1976.
[9] N. Iwashita, J. Field, M. Swain, Indentation hysteresis of glassy carbon materials, Philos. Mag. A 82 (10) (2002) 1873–1881.
[10] N. Iwashita, et al., Elasto-plastic deformation of glass-like carbons heat-treated at different temperatures, Carbon 39 (10) (2001) 1525–1532.
[11] C. Lee, et al., Measurement of the elastic properties and intrinsic strength of monolayer graphene, Science 321 (5887) (2008) 385–388.
[12] A.C. Ferrari, et al., Elastic constants of tetrahedral amorphous carbon films by surface Brillouin scattering, Appl. Phys. Lett. 75 (13) (1999) 1893–1895.
[13] E. Broitman, et al., Structural and mechanical properties of diamond-like carbon films deposited by direct current magnetron sputtering, J. Vac. Sci. Technol. A 21 (4) (2003) 851–859.
[14] S. Amelio, et al., Measurements of elastic properties of ultra-thin diamond-like carbon coatings using atomic force acoustic microscopy, Thin Solid Films 392 (1) (2001) 75–84.
[15] J. Robertson, Properties and prospects for non-crystalline carbons, J. Non-Crystall. Solids 299–302 (2002) 798–804 (Part 2).
[16] Q. Wei, J. Sankar, J. Narayan, Structure and properties of novel functional diamond-like carbon coatings produced by laser ablation, Surf. Coatings Technol. 146–147 (2001) 250–257.
[17] D.W.M. Lau, et al., The structural phases of non-crystalline carbon prepared by physical vapour deposition, Carbon 47 (14) (2009) 3263–3270.
[18] X. Shi, et al., Transport of vacuum arc plasma through an off-plane double bend filtering duct, Thin Solid Films 345 (1) (1999) 1–6.
[19] A.J. Haq, et al., Correlation of nanoindentation-induced deformation microstructures in diamondlike carbon coatings on silicon substrates with simulation studies, J. Mater. Res. 25 (05) (2010) 910–920.
[20] B. Haberl, et al., Phase transformations induced in relaxed amorphous silicon by indentation at room temperature, Appl. Phys. Lett. 85 (23) (2004) 5559–5561.
[21] J.T. Titantah, D. Lamoen, Determination of the electron effective band mass in amorphous carbon from density-functional theory calculations, Phys. Rev. B 70 (3) (2004) 033101.
[22] R. Egerton, Electron Energy-loss Spectroscopy in the Electron Microscope, Springer Science & Business Media, 2011.
[23] W.C. Oliver, G.M. Pharr, An improved technique for determining hardness and elastic modulus using load and displacement sensing indentation experiments, J. Mater. Res. 7 (06) (1992) 1564–1583.
[24] X. Chen, J.J. Vlassak, Numerical study on the measurement of thin film mechanical properties by means of nanoindentation, J. Mater. Res. 16 (10) (2001) 2974–2982.
[25] M. Sakai, The Meyer hardness: a measure for plasticity? J. Mater. Res. 14 (09) (1999) 3630–3639.
[26] G.M. Pharr, W.C. Oliver, Measurement of thin film mechanical properties using nanoindentation, MRS Bull. 17 (07) (1992) 28–33.
[27] G.M. Pharr, et al., Hardness, elastic modulus, and structure of very hard carbon films produced by cathodic-arc deposition with substrate pulse biasing, Appl. Phys. Lett. 68 (6) (1996) 779–781.
[28] W.D. Nix, Elastic and plastic properties of thin films on substrates: nanoindentation techniques, Mater. Sci. Eng. A 234–236 (1997) 37–44.
[29] C. Kocer, An automated incremental finite element study of Hertzian cone crack growth, Finite Elements in Analysis and Design 39 (7) (2003) 639–660.
[30] Spear, Synthetic Diamond — Emerging CVD Science and Technology, Wiley, , NY, 1994.
[31] S.J. Zinkle, L.L. Snead, Thermophysical and Mechanical Properties of SiC/SiC Composites, in Other Information: PBD: Sep 1998; Related Information: Is Part of Fusion materials semiannual progress report for the period ending June 30, 1998; Burn, G. [ed.] [comp.]; PB: 314 pp., 1998, pp. 93–100. p. Medium: X; Size
[32] D.W.M. Lau, et al., Abrupt stress induced transformation in amorphous carbon films with a highly conductive transition phase, Phys. Rev. Lett. 100 (17) (2008) 176101.
[33] P.J. Fallon, et al., Properties of filtered-ion-beam-deposited diamondlike carbon as a function of ion energy, Phys. Rev. B 48 (7) (1993) 4777–4782.
[34] M. Chhowalla, et al., Influence of ion energy and substrate temperature on the optical and electronic properties of tetrahedral amorphous carbon (ta-C) films, J. Appl. Phys. 81 (1) (1997) 139–145.
[35] J. Koskinen, J.-P. Hirvonen, J. Keränen, Effect of deposition temperature and growth rate on the bond structure of hydrogen free carbon films, J. Appl. Phys. 84 (1) (1998) 648–650.
[36] R. Gago, et al., Evolution of s p 2 networks with substrate temperature in amorphous carbon films: experiment and theory, Phys. Rev. B 72 (1) (2005) 014120.
[37] J.M. Jungk, et al., Indentation fracture toughness and acoustic energy release in tetrahedral amorphous carbon diamond-like thin films, Acta Mater. 54 (15) (2006) 4043–4052.
[38] N.A. Marks, Evidence for subpicosecond thermal spikes in the formation of tetrahedral amorphous carbon, Phys. Rev. B 56 (5) (1997) 2441–2446.
[39] M.G. Beghi, et al., Bonding and mechanical properties of ultrathin diamond-like carbon films, Appl. Phys. Lett. 81 (20) (2002) 3804–3806.
[40] J. Philip, et al., Elastic, mechanical, and thermal properties of nanocrystalline diamond films, J. Appl. Phys. 93 (4) (2003) 2164–2171.
[41] M.P. D'Evelyn, T. Taniguchi, Elastic properties of translucent polycrystalline cubic boron nitride as characterized by the dynamic resonance method, Diam. Relat. Mater. 8 (8–9) (1999) 1522–1526.
[42] M. Grimsditch, E.S. Zouboulis, A. Polian, Elastic constants of boron nitride, J. Appl. Phys. 76 (2) (1994) 832–834.

UNCORRECTED PROOF